Journal of Translational Medicine

RESEARCH

Open Access

Bacterial colonization contributes to pathological scar formation via the regulation of inflammatory response

Ning Yang[1†], Hao Zhang[2†], Yuheng Zhang[1,3†], Bin Lin[1], Rong Huang[1], Tingting Cui[4*] and Xueyong Li[1*]

Abstract

Background It has been established that inflammatory factors are involved in the formation of pathological scars. Therefore, pathological scars are regarded to be highly associated with chronic inflammation, whereas what factors contribute to this inflammation remains unclear.

Objective To confirm that bacterial colonization is involved in the formation of pathological scars, and to reveal that the persistent inflammatory response mediated by macrophages due to bacterial colonization promotes scar formation.

Methods This study included 23 normal skin controls and 58 untreated pathological scar samples. To detect the presence of bacteria in surgically-excised scar samples and alterations of histology, as well as bacteria-associated gene levels, histological staining, immunoelectron microscopy, microbiological and cell culture and molecular biology detection methods were employed. The PICRUSt2 tool and BugBase were employed to identify pathways, genes, and phenotypic differences.

Results We found that in pathological scars, bacteria were widely distributed both extracellularly and intracellularly, with intracellular bacteria primarily located in the cytoplasm of macrophages and fibroblasts. A total of 2,260 bacterial species were detected in pathological scars, primarily from the *Clostridiales*, *Burkholderiales*, *Actinomycetales*, and *Bacteroidales* orders. Moreover, the pathogenicity and motility of colonizing bacteria were positively correlated with the degree of scar hyperplasia and invasiveness. The lysates of four clinically-relevant bacterial species had differential effects on the secretion of inflammatory cytokines from macrophages. When treated macrophage supernatant was added to fibroblasts, collagen secretion was dysregulated, and fibroblast differentiation into myofibroblasts prominently increased. In rat scar model, the expression of inflammatory factors and growth factors in the scar tissue was increased, which activated the TGF-β/Smad signaling pathway, resulting in the increasing of α-SMA.

[†]Ning Yang, Hao Zhang and Yuheng Zhang contributed equally to this work.

*Correspondence:
Tingting Cui
cuitt_1210@126.com
Xueyong Li
lixueyong641123@163.com

Full list of author information is available at the end of the article

Conclusions Persistent activation of macrophages by tissue-colonizing bacteria may be a key factor in promoting inflammatory response and dysregulated collagen deposition in pathological scars, offering a potential new strategy for preventing and treating pathological scars.

Keywords Bacterial colonization, Fibroblast, Macrophage, Chronic inflammation, Pathological Scar

Introduction

Pathological scars, which are thought to be the final hurdle in wound healing, are benign fibroproliferative skin tumors [1, 2]. Pathological scar is an excessive tissue response of the body to dermal injury, mainly manifested as immoderate proliferation of fibroblasts, deposition of extracellular matrix, high infiltration of local inflammatory cells, and high dermal vascularization, with or without invasive growth to the surrounding normal skin [3, 4]. Unfortunately, the pathogenesis of scars has still been a challenging problem for both clinicians and researchers [5–7]. Race, skin tension, hormone level, and susceptibility gene have been reported to be associated with the formation of pathological scar. The incidence of pathological scar is different among different races. In China, it ranges from 0.1 to 16.0%, accounting for 0.075–0.123% of all hospitalized patients. The degree of hyperplasia of different scars in the same patient or different segments of the same scar showed enormous heterogeneity.

Chronic inflammation in the dermal reticular layer, considered by some experienced researchers, was fundamental to the pathogenesis of pathological scars [8]. The inflammatory response plays a dual role: on one hand, it accelerates tissue repair by recruiting various cells, but on the other hand, it drives atypical fibroblast proliferation and abnormal deposition of extracellular matrix components like collagen [9]. Existing studies have manifested that proinflammatory factors, such as tumor necrosis factor-α (TNF-α), transforming growth factor-β (TGF-β), interleukin-1 (IL-1) and interleukin-6 (IL-6), as well as immune cells, like macrophages, are enriched in pathological scar tissues, which indicates the persistence of inflammatory responses [10]. As a result, pathological scars are thought to result from chronic inflammation, though why this inflammation occur remains unclear [7]. A clear history of infection greatly increases the risk of developing pathological scars [11, 12]. Some researchers report that pathological scars are secondary to insect bites, skin punctures, vaccines, folliculitis, acne, chickenpox, and shingles infections [13]. Additionally, the bacterial load before epithelialization is positively correlated with the risk of developing pathological scars [14]. According to existing research, pathological scars seem to be related to bacterial infection. Unfortunately, the direct effect of bacterial colonization on the scar remodeling stage is ill-defined [15]. There is no research report on whether the original microorganism is still morbigenous in the skin tissue after wound epithelialization and its effect on pathological scar formation.

This research was designed to find out the evidence of pathogens colonization in human pathological scars and further clarify the mechanism of pathological scar formation, which may provide experimental and theoretical basis for new therapeutic targets.

Materials and methods

Patients and sample collection

Inclusion criteria: scars that are raised above the skin surface; accompanied by pain/itching; recent volume growth with a surface that is red, flushed or purple. Exclusion criteria: presence of chronic underlying diseases; chronic wounds at the scar site; history of scar-related treatment; immunodeficiency diseases; mental illness cannot cooperate with treatment or other conditions that are not suitable for participation in this study. This study totally involved 58 patients (34 females, 24 males, aged 3–76 years) with untreated pathological scars, along with 23 normal skin tissue samples (14 females, 9 males, aged 14–59 years) collected from the surgical area as controls. To prevent contamination, three steps were followed to eliminate environmental, iatrogenic, and experimental contamination. None of them had received any treatments previously. The samples were collected between January 2021 and December 2021 at the Second Affiliated Hospital of Air Force Medical University. This study complied with the guidelines provided by the World Medical Association Declaration of Helsinki on Ethical Principles for Medical Research Involving Humans for studies, and was approved by the Ethics Committee of the Second Affiliated Hospital of Air Force Medical University (No. 202011-33 and 202201-02).

Sample quality control standard

We created three filters to help eliminate environmental, iatrogenic, and experimental contamination. Firstly, the same cryogenic storage tube was used to collect the air in the operating room at the same time as surgical resection and the sample separation to avoid air cross-contamination in the operating room. These air samples were submitted for examination with the tissue sample. Secondly, although disinfection of the surgical area could prevent postoperative infection, the surgical blade could still carry epidermal colonization bacteria to the sample surface. Therefore, after removing the entire scar tissue, subcutaneous tissue and epidermis, a new surgical blade

was replaced to separate the core dermal tissue. After the operation, the separation blade and scar tissues were submerged in the Luria Broth (LB) medium and cultivated for 3 days at 37 °C and 120 rpm. If the blade culture results were positive, it proved that iatrogenic contamination was introduced during the sample separation process, and these samples would not be subjected to further experiments. Thirdly, although the laboratory had strict quality control standards, there was still a possibility of contamination. A sterile saline control group ($n = 10$) was added to the DNA extraction, PCR amplification and sequencing library of each batch sample. The bacterial species in the filters were removed from the sequencing results of each sample.

Animals and agents

SD rats were purchased from Air Force Medical University Animal Experiment Center. OriCell ® human fibroblast cell line was obtained from Cyagen Biosciences (HXXFB-00001). THP-1 cells line was obtained from Procell (CL-0233). *Propionibacterium acnes* (ATCC6919), *Pseudomonas aeruginosa* (ATCC27853), *Klebsiella pneumoniae* (ATCC4352) and *Staphylococcus aureus* (ATCC29213) were obtained from the American Type Culture Collection (ATCC). All animal procedures were approved by the Experimental Animal Ethics Committee of Air Force Medical University.

Bacteria DNA extraction, 16S amplification and deep sequencing

Bacteria DNA was extracted from 58 pathological scar and 23 normal skin tissue samples (dermal tissues using the HiPure Tissue DNA Mini Kit (D3121-02, Magen, Shanghai, China). The sequencing method was based on Nejman et al.'s [16]. and the data were uploaded to the SRA database (BioProject accession number: PRJNA811823). The sequencing results in air samples and sterile saline samples were all eliminated from the tissue samples, and then analyzed. 16S amplification, deep sequencing and data analysis were entrusted to be completed by Lianchuan Biotechnology Co., Ltd (Hangzhou, China).

Real-time quantitative PCR (RT-qPCR)

The V6 region of 16S ribosomal RNA was detected using two bacterial primers. Each reaction used 40 ng of DNA, re-peated three times. DNA was combined with two primers (500 nM) and 10 μL SYBR Green Mix (4472908, Thermo Scientific, Waltham, MA, USA) in a 25 μL reaction system. The RT-qPCR was performed using a Roche LightCycler96 system (Basel, Swiss) at 95 °C for 10 min, followed by 50 cycles of 95 °C for 15 s and 60 °C for 45 s. Select *Pseudomonas aeruginosa* in logarithmic growth period as reference standard, and draw the standard curve between bacterial number and Cq value, which was used to estimate the bacterial load in each sample. Fifty-eight sterile saline samples taken during surgery were used as controls to account for environmental bacterial contamination. The primers' sequences were shown in Supplementary Table 1.

H&E, Masson and Van Gieson staining

Three samples were randomly selected from each group for subsequent experiments (human and SD rat) such as full-layer paraffin sectioning and histological staining. For H&E staining, sections were treated with Mayer's hematoxylin (C0105S, Beyotime, Shanghai, China), followed by eosin (C0105S, Beyotime, Shanghai, China). Sections were dehydrated with ethanol (95%, 100%) and cleared using xylene. MASSON and Van Gieson staining were conducted following the instructions using Masson tricolor staining solution (G1006, Servicebio, Wuhan, China) and Modified Van Gieson Ponceau S stain kit (G1046, Servicebio, Wuhan, China).

Immunohistochemical assays

Paraffin sections of human or SD rats' samples were stained for α-SMA, bacterial Lipoteichoic Acid (LTA) and Lipopolysaccharide (LPS), and paraffin sections of normal skin were stained as control group. The sections were deparaffinized with xylene, rehydrated with ethanol, and incubated in a blocking solution (PBS + 1% BSA) at room temperature for 1 h. After overnight incubation with primary antibodies at 4 °C, immunostaining was performed using an avi-din-biotin-peroxidase complex kit (DAB Peroxidase Substrate Kit, Vector Laboratories, Burlingame, CA, USA). The slides were visualized using a NikonDS-U3 automated slide scanner (DA-U3, Nikon, Shanghai, China).

Immunoelectron microscopy analysis

Scar samples were transferred into an EP tube with fresh IEM fixative (G1124-100ML, Servicebio, Wuhan, Hubei, China) and stored at 4 °C. PBS containing 5% nonfat milk and 0.1% Tween 20 (PBS-MT) was used to block sections. The sections were incubated overnight at 4 °C with specific antibodies against LPS (Lipopolysaccharide Core, mAb WN1 222-5, HycultBiotech, Philadelphia, PA, USA, #HM6011, 1:50 dilution). After washing, slides were incubated with goat anti-mouse IgG conjugated with 10-nm gold particles (G7777, Sigma, St. Louis, MO, USA) for 1 h at 37 °C. Transmission electron microscopy was used to scan the samples (HT7800, HITACHI, Tokyo, Japan).

16S ribosomal ribonucleic acid fluorescence in situ hybridization (16S rRNA FISH)

Pathological scar slides were deparaffinized, rehydrated, and boiled in a retrieval solution for 15 min. The slides were incubated with proteinase K (20 μg/mL, G1205, Servicebio, Wuhan, Hubei, China) for 10 min and then with pre-hybridization solution for 1 h at 37 °C. Cy5-labeled probes at 100 nM were hybridized overnight at 30 °C. After washing, the slides were incubated with DAPI and imaged using a fluorescence microscope (IXplore, Olympus, Tokyo, Japan). The probes' sequences were shown in Supplementary Table 1.

Live in-situ bacteria labeling with fluorescent D-alanine

Three cases were randomly selected from the fresh scar center samples obtained from the above experiments, which were cut into 1 mm thick slices and incubated for 24 h at 37 °C with blue fluorescently labeled D-alanine (HADA, R&D Systems, Minneapolis, MN, USA) or DMSO as a control. After washing, the slices were fixed in 4% paraformaldehyde for 1 day at room temperature and embedded in paraffin. Cross-sectional slices were stained with DRAQ5 (ab108410, Abcam, UK) and scanned using the Pannoramic MIDI automated slide scanner (3D HISTECH, Budapest, Hungary).

Microbiological culture

Pathological scar tissue samples were transported to our laboratory at 4℃ in sterile containers without any medium, cut into small pieces in PBS and finally, grown in the LB medium (Aobox, China, 02-136) at 37 °C with 120 rpm shaking without grinding to avoid contamination. After 3–5 days of culture, smearing, Gram staining and microscopic examination were conducted.

Establishment of the bacterial colonization model

Air Force Medical University's Ethics Committee approved protocols for animal experiments. SD rats (200 ~ 250 g, males) obtained from Experimental Animal Centre of Air Force Medical University, Xi'an, China, were acclimated for four weeks before the experiment. Inhalational anesthesia was used to anesthetize rats with 4% isoflurane for induction and 2% isoflurane for maintenance. After shaving, the back area was disinfected with 75% alcohol. Drew a 4 cm by 3 cm rectangle in the middle of the back.

P. aeruginosa infection group ($n = 3$, ATCC27853), *P. acnes* infection group ($n = 3$, ATCC29213), *S. aureus* infection group ($n = 3$, ATCC6919) and *K. pneumoniae* infection group ($n = 3$, ATCC4352) were randomly selected, with saline solution control group ($n = 3$). Bacteria were washed with normal saline twice (1000 rpm, 5 min) to prepare a bacterial suspension with OD600nm = 0.6. The bacterial solution (3 ml per animal) was injected into the dermis of the rat back using 1/2 cc U-40 insulin syringes. All injection operations were performed by the same surgeon. The full-thickness skins were photographed and sampled at days 0, 7, 14, 28, respectively.

Preparation of bacterial lysate

Bacteria, including *P. acnes*, *S. aureus*, *K. pneumoniae*, and *P. aeruginosa*, were amplified, centrifuged at 1500 rpm for 5 min, and lysed using enzymes and ultrasound in an ice bath. The BCA protein concentration standard curve was used to prepare the bacterial lysate. The bacterial lysates were diluted to a protein concentration of 50 μg/mL.

Cell culture

THP-1 cells were cultured in THP-1 special medium (CM-0233, Procell) and human primary fibroblasts were cultured in DMEM complete medium (PM150210, Procell). THP-1 cells were first planted in the upper layer of the 0.4-micron-diameter Transwell Chamber (CORNING) and 100 ng/ml PMA(Phorbol 12-myristate 13-acetate, BioGems) was added for 48 h to induce adhesions, after reaching logarithmic growth stage, treated with bacterial lysates for 24 h. After elution, human primary fibroblasts were seeded into the lower layer and cultured for 48 h.

Protein extraction and Immunoblotting analysis

After cells were lysed with RIPA buffer (Beyotime) containing PMSF, protein concentrations were determined using a BCA assay kit (Solarbio). Proteins were separated by 10% SDS-PAGE, transferred to PVDF membranes, and blocked with 5% skim milk for 1 h. The membranes were incubated with primary antibodies, and then probed with HRP-conjugated secondary antibodies. Enhanced chemiluminescence substrate (Millipore) was used for visualization. Antibodies were presented on Supplementary Table 1.

Toxicity testing of bacterial lysate

The CCK-8 reagent kit (Topscience, Shanghai, China) was used to detect the toxicity of four bacterial lysates on THP-1 cells. The detection time points were set as the 0th, 1st, 3rd, 5th, and 7th days.

Cell migration assay

A scratch test was conducted to assess the impact of supernatant of THP-1 cells treated with bacterial lysates on skin fibroblast migration. Cells were scratched in the lower layer of Transwell Chamber using a pipette tip, and serum-free DMEM medium was added. Cell migration was observed using an optical microscope.

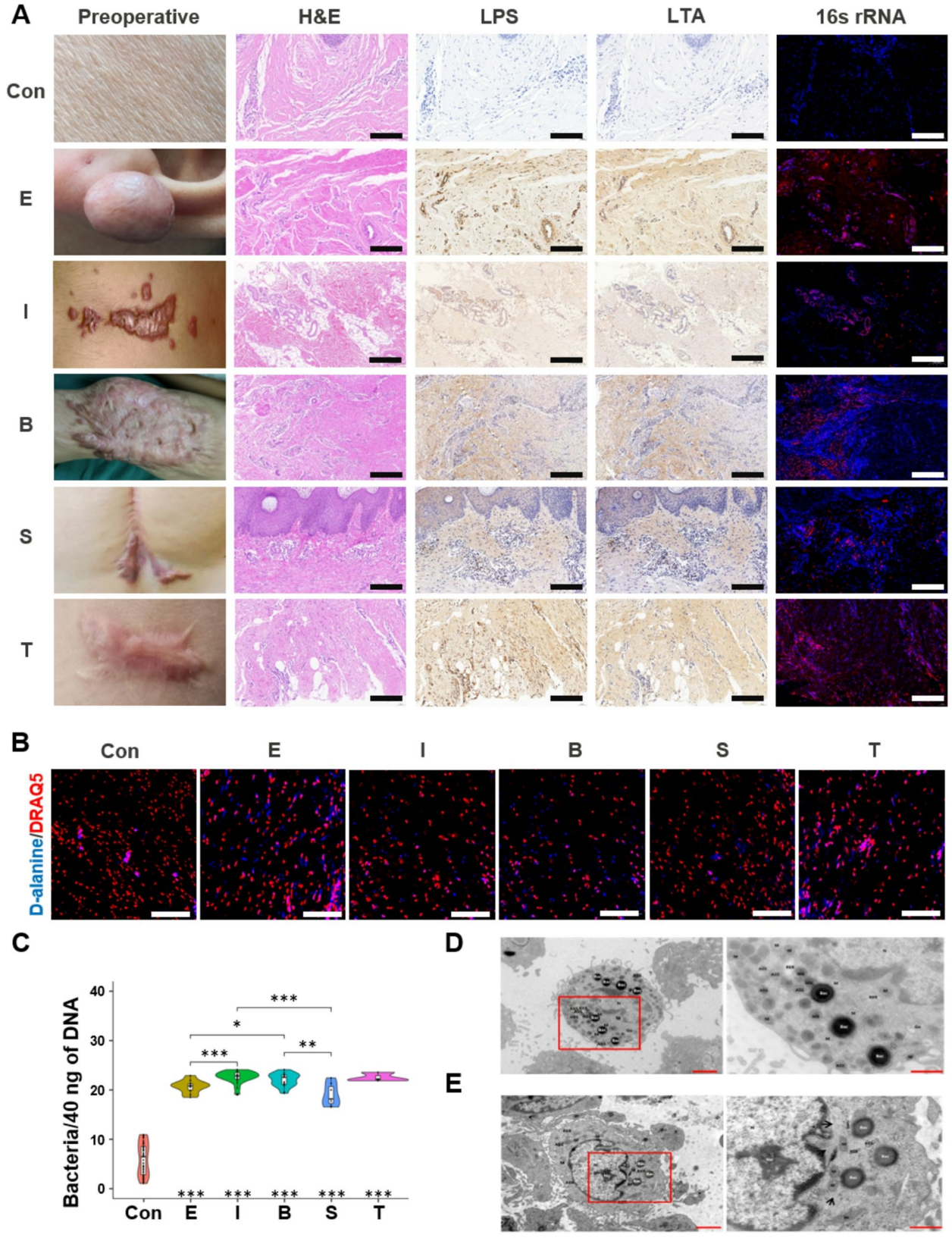

Fig. 1 (See legend on next page.)

(See figure on previous page.)

Fig. 1 Bacterial DNA, RNA, Lipopolysaccharide and Lipoteichoic Acid were Present in pathological scar. (**A**) HE staining, LPS immunohistochemistry, LTA immunohistochemistry, and 16 S rRNA FISH staining for human pathological scar samples. Scale bars, 100 μm; (**B**) In situ bacterial culture and staining results from human pathological scar tissue. Scale bars, 50 μm; (**C**) Bacterial load in scar tissue from different pathogenic factors. t-test, * $p < 0.05$, ** $p < 0.01$, *** $p < 0.001$, the same below; (**D&E**) Bacteria within macrophages (**D**) and fibroblast (**E**), and bacterial composition in pathological scars. Nucleus (N), microbody (MB), Golgi apparatus (Go), mitochondrion (M), microfilament (black arrow), autoph vacuole (AV), rough endoplasmic reticulum (RER), bacteria (Bac). Scale bars, 2 μm and 1 μm

ELISA assay

ELISA was carried out in accordance with instruction of ELISA Kit, including human IL-1 ELISA Set (Mlbio, ml058034), human IL-6 ELISA Set (Mlbio, ml058097), human TNF-α ELISA Set (Mlbio, ml077385), human TGF-β1 ELISA Set (Mlbio, ml022522-2), Rat IL-1 ELISA Set (Sinobestbio, YX-091201R), rat IL-6 ELISA Set (Sinobestbio, YX-091209R). To the THP-1 cells in the upper layer of the Transwell Chamber, the supernatants of that were collected to measure IL-1, IL-6, TNF-α, and TGF-β1 using the commercial ELISA kit (Pierce, Rockford, IL, USA) when cultured for 48 h after treatment with bacterial lysates for 24 h. Bio-antibody and isolated tissue homogenate were added to 96-well plates pre-coated with antibody and incubated at 37 °C, respectively. 60 min later, discarded the liquid, washed the plates completely, and then streptavidin-HRP was added and incubated at 37 °C for 30 min. To avoid light exposure, poured chromogen solution into each well and preserved for 15 min at 37 °C after washing completely. Lastly, infused stop solution into each well and then measured absorbance at 450 nm. There were no bacteria or bacterial lysate in the control group. All the samples were tautologically measured 3 times.

Statistical analysis

Statistical analyses were conducted using GraphPad Prism 8.0.1. Quantitative data are expressed as mean ± standard deviation (SD) from a minimum of three independent experiments. Comparisons between two groups were performed using Student's t-test, while one-way ANOVA with Bonferroni post hoc analysis was applied for multiple group comparisons. A p-value < 0.05 was considered statistically significant.

Results

Bacteria emerges in pathological scars

The 58 samples were divided into five groups based on the underlying cause: ear piercing (E), burns (B), infections (I), surgeries (S), and trauma (T). To label the proteins and nucleic acids of colonized bacteria, LPS was used as a marker for Gram-negative bacteria, and LTA was used for Gram-positive bacteria [17]. Highly-conserved 16S rRNA sequences were also selected for FISH [18]. The staining revealed that numerous bacteria were scattered throughout the pathological scar tissue (Fig. 1A). As D-alanine is exclusively used by bacteria for peptidoglycan synthesis and not by mammalian cells, we further confirmed the presence of live bacteria by culturing scar sections in vitro with fluorescently labeled D-alanine or DMSO. This revealed active bacterial biosynthesis in the scar tissue, with bacteria distributed around the nuclei (Fig. 1B). To quantify the bacterial load, we extracted 40 ng of total DNA from each sample and performed RT-PCR. Using Pseudomonas aeruginosa as a reference, we found between 1 × 10^5 and 10 × 10^5 bacteria per 40 ng DNA in the scar tissue, with the highest bacterial load in the infection-related group and the lowest in the surgical group (Fig. 1C). Further structural analysis using immunoelectron and transmission electron microscopy confirmed that intracellular bacteria were free-floating in the cytoplasm. Macrophages showed mild edema with intact membranes and pseudopod projections. Their nuclei exhibited irregular contours, heterochromatin aggregation, and focal membrane discontinuities. Mitochondria demonstrated localized matrix pallor and swelling, while RER displayed ribosome-rich cisternae. Abundant microbodies and autophagolysosomes were present, along with numerous L-type bacterial variants (lacking cell walls) distributed within the cytoplasm (Fig. 1D). In contrast, fibroblasts displayed intact membranes with abundant microvilli, homogeneous cytoplasmic matrices, and organized microfilament bundles. Organelles were sparse, though mitochondria exhibited uniform size, dense matrix, and parallel cristae. Nuclei contained predominantly euchromatin with preserved membranes, accompanied by occasional rough endoplasmic reticulum (RER) with ribosomes and rare autophagolysosomes (1 per field). Minimal cytoplasmic bacteria were observed (Fig. 1E).

No unique colonizing bacteria cause the formation of pathological scars

Due to the low bacterial load and high species diversity in the scar tissue, we employed 5R 16S sequencing, which involves PCR amplification and sequencing of five regions on the 16S rRNA gene. The Jaccard similarity index quantifies the similarity between two sets by comparing the ratio of their intersection to their union. This metric is widely applied in biology to assess genetic or species similarities [19]. Alpha diversity measures the diversity within a single sample or habitat, capturing species richness, evenness, and dominance. It is a fundamental concept in ecology, microbiology (e.g., microbiome

research), and bioinformatics [20]. The Shannon Index (or Shannon diversity index) evaluates diversity by incorporating both species richness (the number of species) and evenness (the distribution of individuals among species) [21]. Comparing the Jaccard similarity index of scars from different etiologies revealed that scars of the same etiology tended to have more similar bacterial communities (Fig. 2A). Alpha diversity measures, including observed species count and Shannon index, were used to describe the diversity within each sample. Scar tissues contained bacterial species with the types between 27 and 241 (Fig. 2B), and there were no significant differences in the number of bacterial genera across different etiologies. The Shannon index indicated relatively high bacterial diversity in all scar samples, with no statistical difference between groups (Fig. 2C). A total of 2,647 colonized bacteria were detected, 2,646 of which were found in burn samples. 680 bacteria were unique to the burn group. Across the five groups, 18 species of bacteria were detected (Fig. 2D), but this does not indicate the uniqueness of the colonizing species cause pathological scars. We inferred that the occurrence of pathological scars is

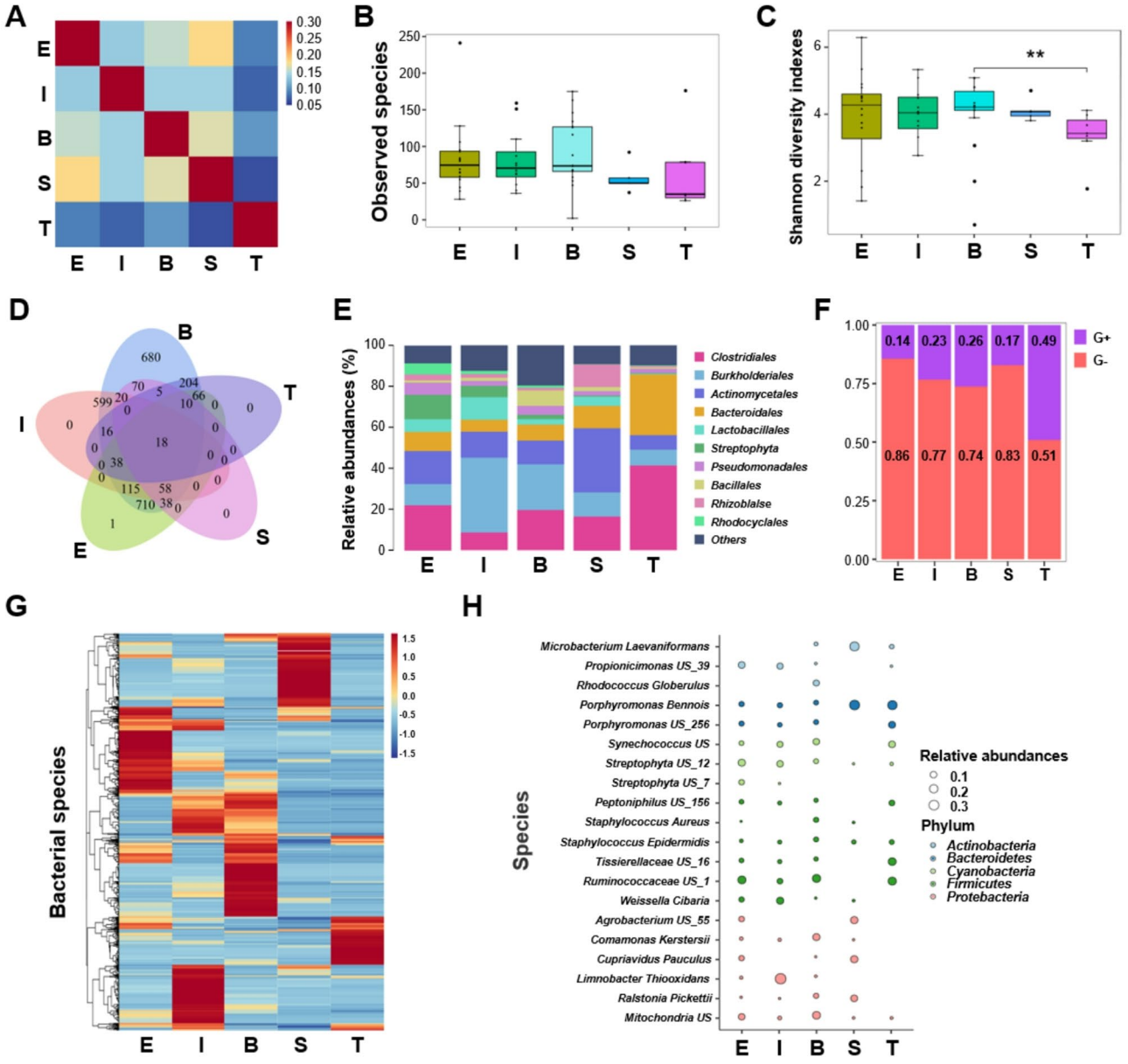

Fig. 2 Human pathological Scars have different microbial compositions. (**A**) Jaccard similarity index analysis; (**B**) Analysis of observed species; (**C**) Alpha diversity of bacterial communities. t-test, $p < 0.01$; (**D**) Wayne diagram of overlapping species across groups; (**E**) Bacterial species distribution by genus; (**F**) Proportions of Gram-negative and Gram-positive bacteria; (**G**) Heatmap of bacterial species distribution; (**H**) Relative abundance of dominant bacterial species

a common pathological manifestation caused by bacterial colonization. At the genus level, the top 10 most abundant genera included *Porphyromonas*, *Ruminococcaceae*, *Comamonas*, *Limnobacter*, *Microbacterium*, *Anaerococcus*, *Staphylococcus*, *Weissella*, and *Pseudomonas*. Significant differences in dominant genera were observed across groups: *Pseudomonas* dominated the infection group, *Microbacterium* the trauma group, and *Porphyromonas* the surgical group (Fig. 2E). Gram-negative bacteria predominated in most groups, except in the trauma group where Gram-positive and Gram-negative bacteria were found in nearly equal proportions (Fig. 2F and G). At the species level, the top 20 most abundant strains included *Microbacterium laevaniformans*, *Propionibacterium sp.*, *Rhodococcus globerulus*, *Porphyromonas benois*, and *Staphylococcus aureus* (Fig. 2H).

The correlation between bacteria and clinical manifestations of scars

To assess the potential impact of colonized bacteria on scar tissue functions and metabolic processes, we used PICRUSt2 software (https://github.com/picrust/picrust2) to compare gene sets with the KEGG database, removing redundant gene sets. MetaCyc pathways were enriched in cases where the expression level exceeded 10%, resulting in 391 MetaCyc pathways (Fig. 3A). Our results indicated that the degree of scar hyperplasia in the ear piercing, infection-related, and burn groups was significantly higher than in the surgical and trauma groups (Fig. 3B). This suggests a positive correlation between the severity of hyperplasia and the pathogenic potential of colonized bacteria, which may explain differences in scar proliferation across different regions of the same patient. Infiltrative growth, another characteristic of pathological scars, was also more pronounced in the trauma and infection-related groups compared to the surgical group (Fig. 3C). A comparative analysis of the scars in burn group or infection-related group and the scars in surgery group was performed. The results showed the scars of surgery group had a significantly higher abundance of motility-related genes in the colonized microorganisms than those of burn group or infection-related group, and the colonized microorganisms in groups could synthesize to varying degrees, including vancomycin, streptomycin, and tetracycline (Fig. 3D and E). The synthesis of antibiotics by colonized bacteria may lead to resistance, rendering clinical treatments less effective. We found that 28% of colonized bacteria in pathological scars were aerobic, 27% were anaerobic, and the remainder were facultative anaerobes (Fig. 3F). When analyzing metabolic pathways, we discovered that certain bacteria in dark red or deep red scars—especially in the ear piercing, burn, and infection-related groups—could synthesize melanin, while no such ability was found in the surgical group (Fig. 3G).

Different bacteria promoted the expression of inflammatory factors in different stages

According to the 16S sequencing results and the actual situation of nosocomial infection, *S. aureus*, *P. aeruginosa*, *K. pneumoniae* and *P. acnes* were selected for in vivo and in vitro experiments. These four kinds of bacteria at logarithmic growth stage were re-suspended into OD600 nm = 0.6 bacterial suspension with normal saline and intradermal injection was intravenously conducted into the back skin of SD rats. Continuous macro photography indicated that the inflammatory reaction reached its peak on the 7th day, and the appearance showed obvious redness and swelling, accompanied by differing degrees of epidermal exfoliation (Fig. 4A, red arrow).The skin lesions were progressively restored over time, and the most severe lesions were caused by *P. acnes*. Pathological sections at different time points demonstrated that when the inflammatory reaction caused by bacteria was restricted to the subcutaneous tissue, it had little effect on the dermis. Once the inflammatory reaction breaks through the junction of subcutaneous tissue and dermal reticular layer, it will gradually spread to the epidermis until it penetrates the whole skin layer (Fig. 4B). And in a large number of sections, there was no acute inflammatory response that confined to the dermis. This was consistent with that pathological scar inflammation can reach to the depth of dermal reticular layer and fibroblasts within the scar can migrate from the subcutaneous fascia. We detected the content of IL-1 and IL-6 in the skin tissues of rats before and after the injection of bacterial lysates, and we found that the four kinds of bacteria all promoted the expression of IL-1 at different time points. On the other hand, bacteria like *P. acnes* also promoted the expression of IL-6 (Fig. 4C and D). In order to further prove the stimulating effect of bacteria on rat skin fibroblasts, we added four kinds of bacterial lysates at 25 μg/mL, 50 μg/mL and 100 μg/mL into the culture medium of rat skin fibroblasts. The results revealed that after 2 h, IL-1 and IL-6 in supernatant began to increase, and reached the peak at 3–5 days (Fig. 4E and F). We found that the lysate of *S. aureus* did not induce significant changes in IL-6, and the results were same in vivo. Due to the different virulence of different bacteria lysates, the expression of IL-1 and IL-6 indicated different concentration dependence.

Biological effects of bacterial lysates on THP-1 and human primary skin fibroblasts

Macrophages and fibroblasts have been highly valued in the study of scar pathogenesis due to their secretion functions of various cytokines and extracellular matrix. To investigate the biological effects of colonized bacteria on THP-1 cells and human primary skin fibroblasts, we selected *P. acnes*, *P. aeruginosa*, *K. pneumoniae*, and

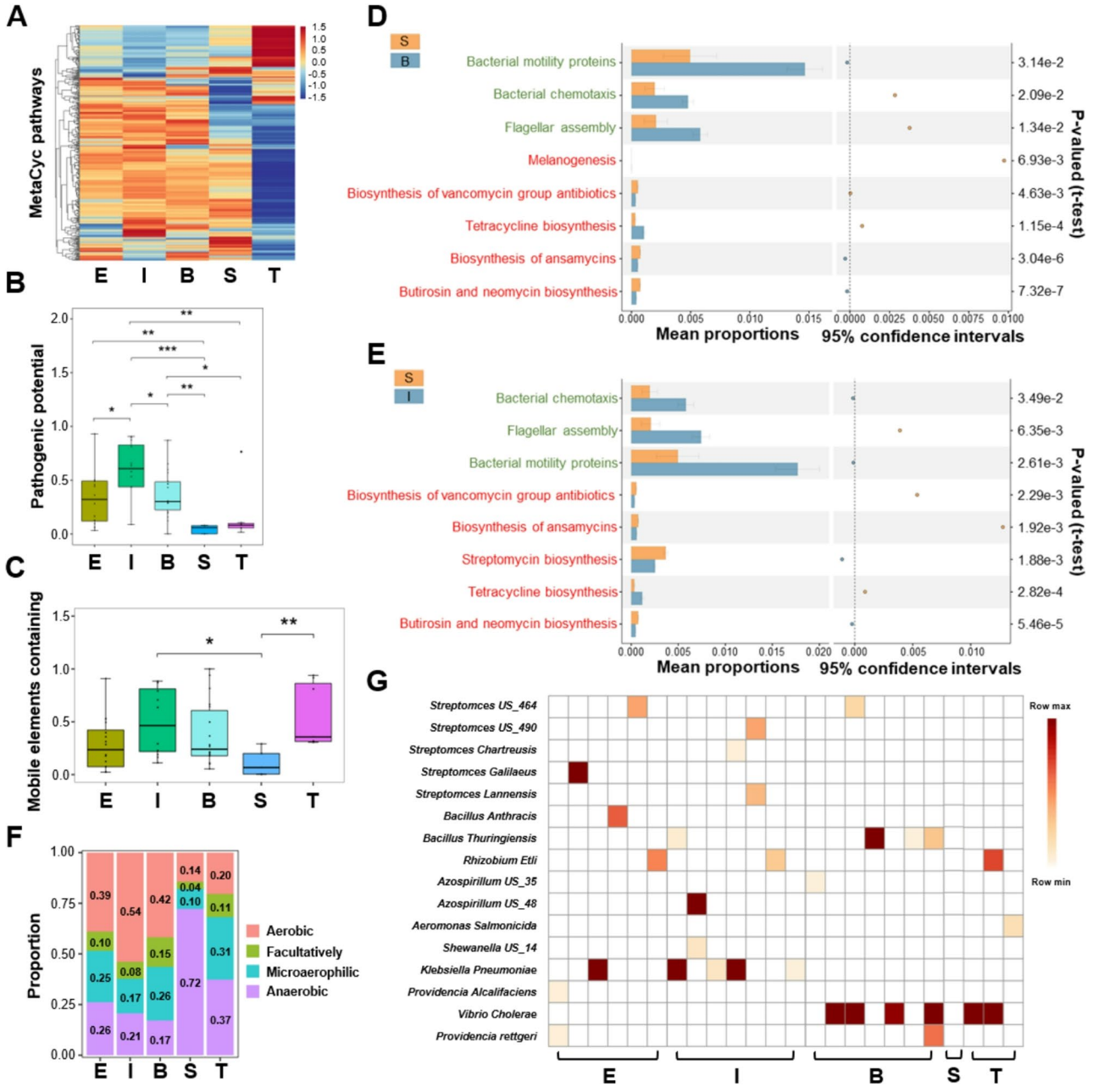

Fig. 3 Metabolic functions encoded by bacteria are connected with the clinical manifestations of heterogenes. (**A**) Hierarchical clustering heatmap of 391 MetaCyc pathways; (**B**) Box plot of bacterial pathogenic potential; (**C**) Box plot of mobile element content in bacterial communities; (**D**, **E**) Pathways related to antibiotic synthesis (red) and motility (green); (**F**) Proportion of aerobic, anaerobic, and facultative anaerobic bacteria; (**G**) Heatmap of melanin-producing bacteria

S. aureus for in vitro experiments based on sequencing results and their known pathogenicity in clinical infections (Fig. 5A). Bacterial lysates were prepared from logarithmic phase bacterial cultures, centrifuged, and washed before being added to THP-1 cell cultures at 50 μg/mL. Cells were cultured at 37 °C with 5% CO_2 for 1, 3, 5, and 7 days for CCK-8 toxicity and proliferation assays. The results indicated that the toxicity of the bacterial lysates varied, with *P. acnes* exhibiting the weakest toxicity. The inhibition of cell growth was time-dependent, with longer exposure resulting in greater toxicity (Fig. 5B). A scratch test was performed to assess the effect of supernatant of THP-1 cells treated with bacterial lysates on fibroblast migration. *S. aureus* group inhibited fibroblast migration, while *P. aeruginosa* group promoted it, with statistically significant differences (Fig. 5C and D). To assess the direct impact of bacterial lysates on THP-1 cells, the levels of IL-1, IL-6, TNF-α and TGF-β1

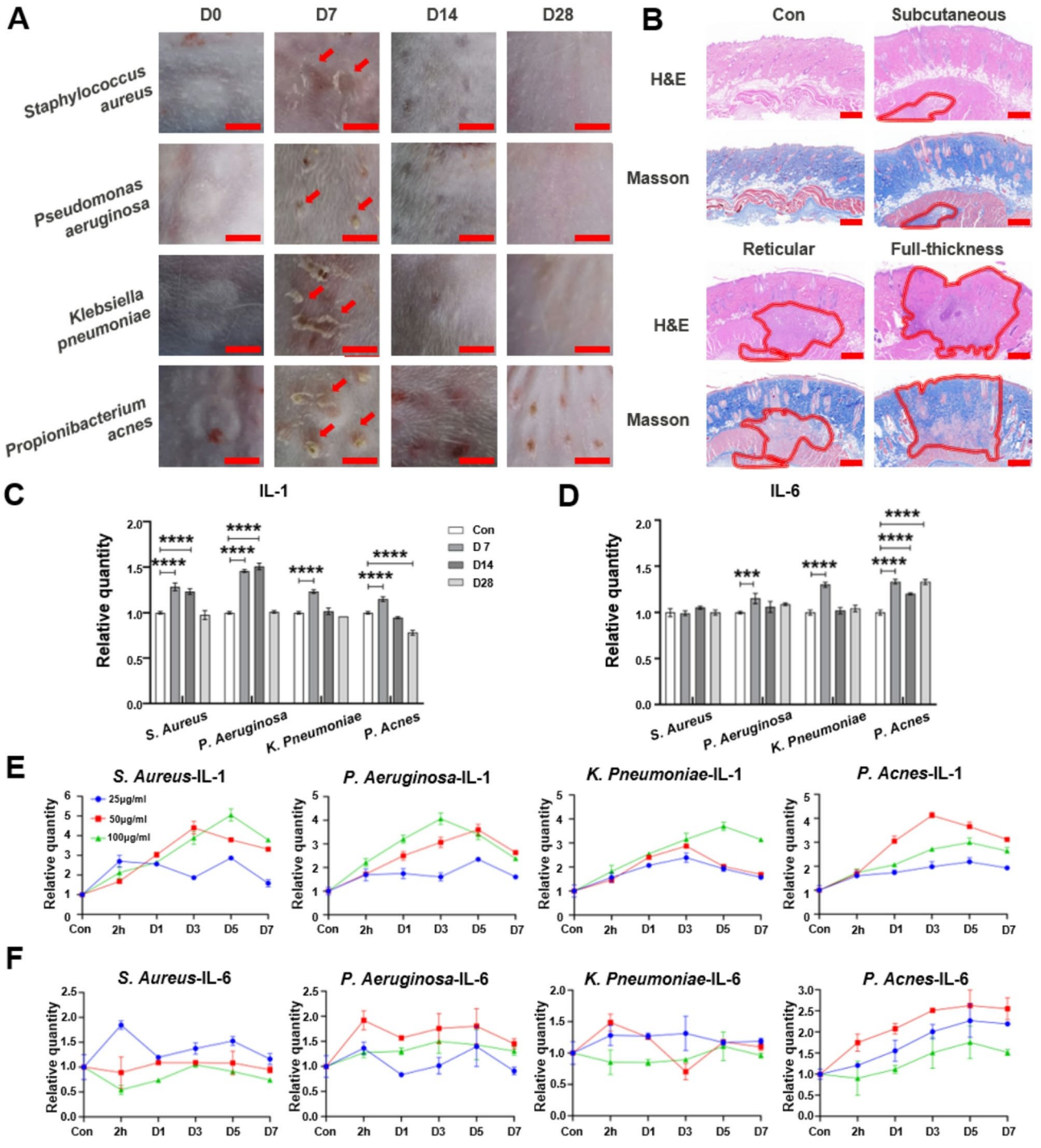

Fig. 4 Bacteria can promote the expression of inflammatory factors at different time points. (**A**). Macroscopic images of dorsal skin of SD rats after injection of bacteria. Scale bars, 5 mm. (**B**). Successive sections showing inflammatory infiltration were stained with H&E and Masson. The area circled in red is the site of inflammation. Scale bars, 500 μm. (**C&D**). Bar chart shows the variation trend of IL-1 (**C**) and IL-6 (**D**) in the skin of SD rats that contains four types of bacteria over time. ($n = 3$, Tukey's multiple comparisons test) (**E.&F**). The line chart shows the changes of IL-1 (**C**) and IL-6 (**D**) expression in dorsal skin of SD rats after injection of four kinds of bacteria over time. ($n = 3$, Tukey's multiple comparisons test)

in supernatants were detected by ELISA. The results showed an increase in these factors at early stages, followed by depletion over time (Fig. 5E). After co-culture with THP-1 cells treated with four bacterial lysates, the expression of α-SMA increased and the ratio of Col I/Col III decreased in human primary fibroblasts (Fig. 5F-I). The results suggest that bacterial lysate can affect the growth of fibroblasts and extracellular matrix secretion

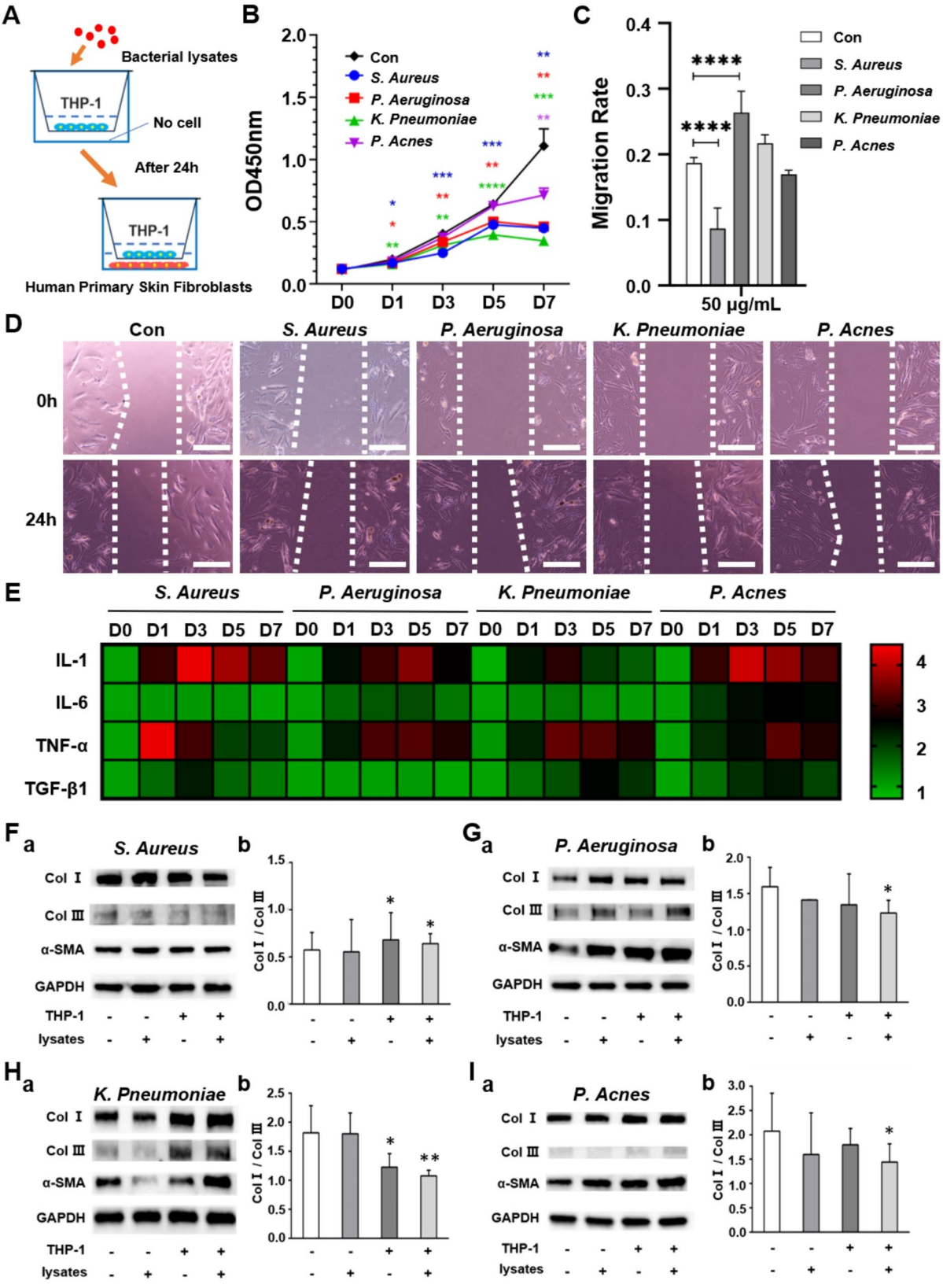

Fig. 5 (See legend on next page.)

(See figure on previous page.)

Fig. 5 Bacterial lysate can affect the growth of fibroblasts and extracellular matrix secretion by influencing the secretion of various cytokines. (**A**) Schematic diagram of cell culture in Transwell Chamber; (**B**) CCK-8 toxicity results for THP-1 cells treated with bacterial lysates. Using Tukey's mul-tiple comparisons test to calculate p-values; (**C**) Bar chart of migration analysis, with statistical significance. Using Tukey's multiple comparisons test to calculate p-values; (**D**) Cell migration assay's results of fibroblast migration in response to supernatant of THP-1 cells treated with bacterial lysates. Scale bars, 200 μm; (**E**) The levels of IL-1, IL-6, TNF-α, and TGF-β1 in the supernatants following exposure to bacterial lysates; (**F-I**) (a) Western blotting pictures. (b) Relative ratio of Col I/Col III. (The bacterial lysates in F-I were S. aureus, P. aeruginosa, K. pneumoniae and P. acnes, respectively)

by influencing the secretion of various cytokines by macrophages, and may play an important role in the mechanism of scar formation.

Bacteria stimulated transdifferentiation of skin fibroblasts to myofibroblasts

In human pathological scar samples, we found that fibroblasts at the site of bacterial deposition would highly express α-SMA, and collagen fibers would also transform into muscle fibers (Fig. 6A). Thus, we injected four kinds of bacteria into the skin in the back of rats and observed for 28 days, and we found the same results (Fig. 6B). To further explore the mechanism, we detected the expression levels of TGF-β1 and TNF-α in rats tissues, and found that four kinds of bacteria can all promote the expression levels of TGF-β1 and TNF-α in different degrees, among which *P. acnes* had the most significant promoting effect (Fig. 6C). The expression levels of TGF-β1 and TNF-α αnd peak time were different due to the different virulence and intensity of immune response induced by different bacteria. It has been shown that TNF-α binding to receptors can promote the expression of TGF-β1, which binds to receptors activates the Smad family and promotes the expression of α-SMA. So, the western blot analysis was used to detect the changes of Smad3 and α-SMA expression stimulated by *P. aeruginosa* and *P. acnes* over time, and the results showed that the expression increased over time (Fig. 6D and E). In order to prove that bacteria directly promote the transdifferentiation of fibroblasts into myofibroblasts, we added four bacterial lysates into rat skin fibroblasts culture medium at 25 μg/ml, 50 μg/ml and 100 μg/ml. TNF-α in supernatant was significantly increased at 2 h, while TGF-β1 expression peaked at 3–5 days (Fig. 6F and G).

Discussion

Pathological scarring occurs when wound repair progresses beyond epithelialization into persistent inflammation and proliferation, causing tissue hyperplasia and invasion of healthy skin. Common triggers include infections, burns, surgeries, and trauma. In China, ear piercings performed in non-sterile settings (e.g., barbershops) frequently lead to pathological scars with characteristic anatomical patterns, justifying their separate classification. The underlying mechanism involves chronic reticular dermal inflammation, with sustained expression of IL-1α, IL-6, TNF-α [22–24] and elevated CCL/CXCL chemokines [25, 26]. This induces substantial inflammatory cell infiltration [27–29], altering extracellular matrix deposition. Local hypoxia from metabolic activity further stimulates angiogenesis, sustaining chronic inflammation. Despite complex pathogenesis, scar tissue composition remains relatively simple, primarily characterized by type I/III collagen ratios and fibroblast differentiation states. Although chronic inflammation in pathological scars has been increasingly studied, its fundamental origin remains elusive, hindering both mechanistic understanding and targeted therapy development.

While prior studies indicated bacterial clearance post-epithelialization [22], persistent inflammation (erythema, edema, hyperthermia, pain) in pathological scars suggested potential bacterial colonization. Our multi-method investigation confirmed bacterial presence via 16S rRNA sequencing and detection of LPS/LTA proteins. Sterile saline controls excluded environmental contamination. Immunofluorescence and TEM revealed bacteria dispersed throughout scar tissue [30], including wall-deficient intracellular forms resembling L-type bacteria [31], which may be misinterpreted as vesicles. Through 16S amplification and deep sequencing, we found that over 99% of bacteria in pathological scars belonged to five phyla: Bacteroidetes, Proteobacteria, Actinobacteria, Firmicutes, and Cyanobacteria. The first four phyla are typical skin, gut, and oral microbiota [32–35]. Similar to gut and skin microbiomes, scar bacterial communities showed low phylum-level but high species-level diversity [32]. These bacteria likely originated from skin surfaces, hair follicles, sweat glands, or external contaminants during wound healing, persisting in granulation tissue post-epithelialization despite immune defenses.

Microbiome analysis identified 2,648 bacterial species, with 18 colonizers including Staphylococcus epidermidis, Porphyromonas bennonis, and Streptomyces. The absence of universal colonizers suggests bacterial colonization itself (rather than specific species) triggers inflammation. This may explain clinical heterogeneity in scar characteristics (hyperplasia, invasion, morphology, hypoxia, drug resistance) and variations between/within scars. Ear-piercing scars dominated by Clostridiales and Actinomycetales, which is associated with biofilm-forming commensals from ear/nasal flora. Traumatic scars enriched in Clostridiales and Bacteroidales, which

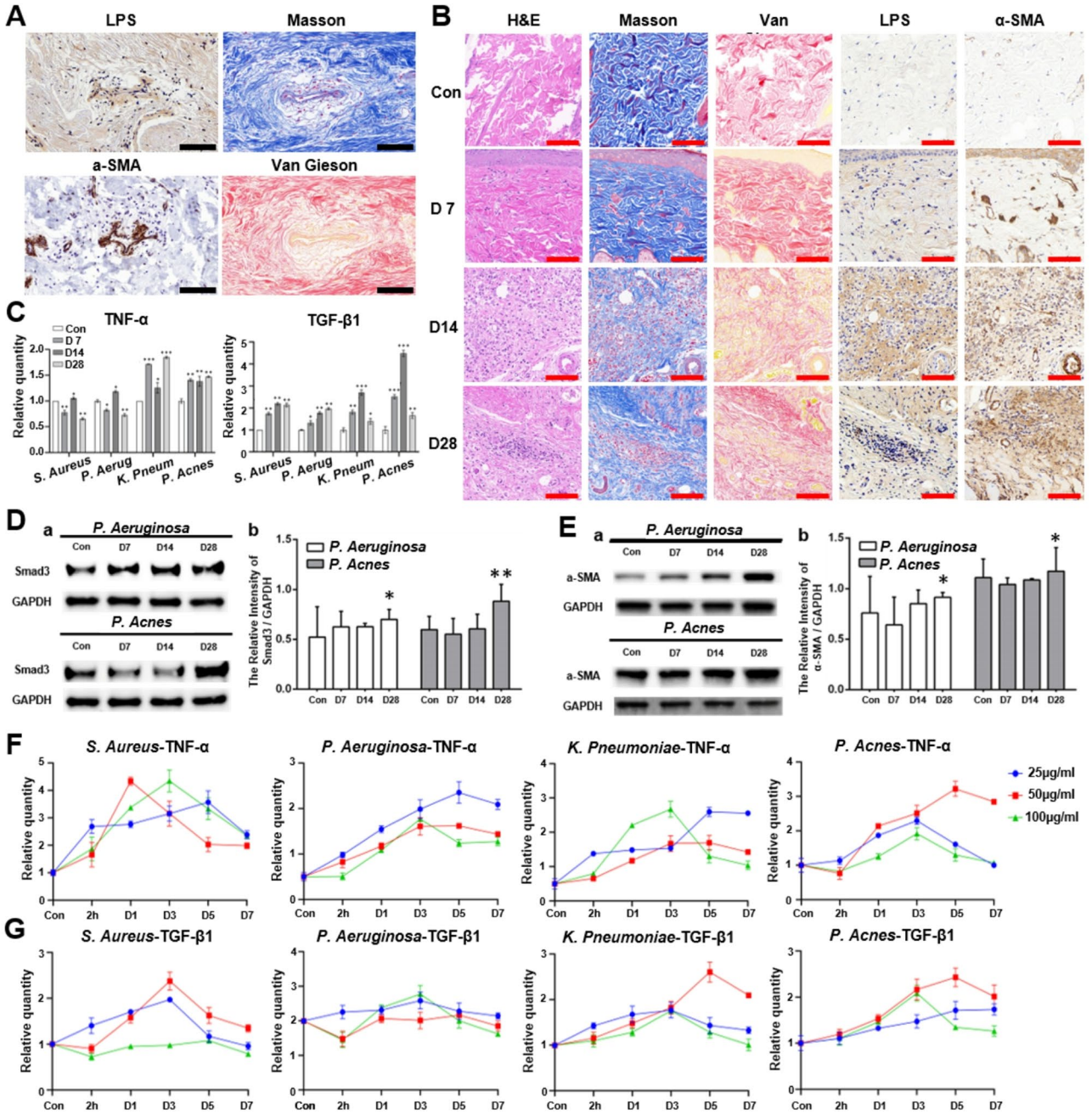

Fig. 6 Bacteria stimulated transdifferentiation of skin fibroblasts to myofibroblasts. (**A**). Consecutive slices from human pathological scars were stained with IHC (LPS, α-SMA), Masson, or Van Gieson. Scale bars, 100 μm. (**B**). Consecutive slices from SD rat dorsal skin with *Pseudomonas aeruginosa* were stained with H&E, Masson, Van Gieson, or IHC (LPS, α-SMA). Scale bars, 100 μm. (**C**). Bar chart shows the variation trend of the contents of TNF-α and TGF-β1 in the skin of SD rats that contained four types of bacteria over time. ($n = 3$, Tukey's multiple comparisons test). (**D&E**). Western blot analyses of full thickness skin tissue were performed to detect Smad3 (**D**) and α-SMA (**E**). β-Actin served as loading control. (**F&G**). The line chart shows the changes of TNF-α (**F**) and TGF-β1 (**G**) expression in human skin fibroblasts stimulated by four bacterial lysates over time. ($n = 3$)

reflects environmental contaminants from initial injury. Surgical scars dominated by high Actinomycetales, which suggests iatrogenic inoculation from sebaceous glands. The distribution of each phylum in burn scars is more balanced, it is worth noting that the proportion of Firmicutes is higher than others. The proportion of Burkholderiales in post-infection scars was extremely high, and the proportion of Lactobacillales was also higher than that other groups, which was also in line with the high lactate environment of infection.

Notably, intracellular bacteria are known to influence tumor metastasis, immune regulation, and metabolism

[36, 37]. Investigating bacterial functions in pathological scars may reveal novel pathogenic mechanisms. These hyperproliferative scars share characteristics with non-metastatic benign tumors [38]. BugBase analysis revealed higher bacterial pathogenicity and motility in surgical scars compared to burn or infection-related scars, correlating with scar proliferation severity. PICRUSt2 predicted enriched pathways (collagen metabolism, TLR signaling, oxidative stress) promoting hyperplasia via ECM dysregulation, chronic inflammation, and oxidative damage. Bacterial migration - either free or within immune cells - may spread inflammation to adjacent tissue, inducing aberrant fibroblast activation and collagen dysmetabolism [39, 40]. Notably, antibiotic production in microorganisms primarily reflects ecological competition, with antibiotic-producing bacteria typically harboring corresponding resistance genes - insights that could inform targeted anti-infection strategies to minimize scarring. These findings suggest pathological scars arise from chronic bacterial inflammation rather than tumor-like processes. Persistent bacterial colonization sustains macrophage activation, spreading inflammation to adjacent tissue and promoting fibroblast activation, excessive ECM deposition, and α-SMA expression. The scar's complex microenvironment and bacterial diversity significantly influence clinical presentation. Intriguingly, pathological scars exhibit aerobic glycolysis resembling the tumor-associated Warburg effect [41, 42]. Scar microbiota analysis revealed only 28% aerobic and 27% anaerobic bacteria. In hypoxic scar tissue, aerobic bacteria may exacerbate hypoxia, while intracellular anaerobes/facultative anaerobes could mimic aerobic glycolysis by altering cellular respiration. Notably, colonizing bacteria produced antibiotics (vancomycin, streptomycin, tetracycline), potentially inducing local resistance and compromising therapeutic efficacy through endogenous antibiotic synthesis.

Pathological scars frequently exhibit erythematous or purpuric discoloration due to neovascularization and inflammation-induced vasodilation. Pigment-producing dermal bacteria may intensify this hyperpigmentation. Bacterial colonization sustains macrophage activation, elevating pro-inflammatory cytokines (IL-1, IL-6, TNF-α, TGF-β1). IL-1 promotes scarring via NF-κB/MAPK pathways [43], while IL-6 exacerbates fibrosis through fibroblast growth factors and enhances neutrophil/monocyte recruitment, amplifying local inflammation [44]. Bacterial stimulation significantly upregulated TGF-β1 expression, activating the Smad pathway and increasing α-SMA levels, thereby promoting fibroblast-to-myofibroblast transdifferentiation [45, 46]. These α-SMA + myofibroblasts excessively produced collagen I/III and metalloproteinase inhibitors, leading to pathological ECM accumulation and tissue contracture. While normally reversible, persistent inflammatory stimuli (IL-1β, TNF-α) or mechanical stress sustained myofibroblast activation. Importantly, we demonstrated persistent bacterial colonization throughout scar formation, challenging previous assumptions of transient influence.

Transwell assays revealed differential fibroblast migration following macrophage activation by distinct bacterial lysates, likely attributable to variant cytokine profiles. Certain lysates enhanced fibroblast proliferation, collagen secretion, and transdifferentiation via macrophages, potentially exacerbating fibrosis. Notably, while infected fibroblasts showed no overt structural changes, colonized macrophages exhibited edema and abundant autolysosomes, suggesting active bacterial invasion when host membranes remain intact. Although this study employed lysates, future work should compare live bacteria's effects. Fibroblasts may also directly respond to infection through TLR-mediated signaling [47]. LPS, a Gram-negative bacterial endotoxin, is known to trigger human fibrotic disorders by activating fibroblast TLR4 signaling, thereby promoting scar formation [48, 49]. This study employed bacterial lysates rather than live bacteria, demonstrating correlation but not causation between bacterial components and scar formation. We are currently conducting in-depth investigations using attenuated bacterial strains and optimized immune cell co-culture systems, which should better elucidate the tripartite interactions among bacteria, immune cells, and fibroblasts. The specific effects of intracellular bacteria on fibroblasts require further exploration.

Wounds provide ideal conditions for bacterial biofilm formation, which promotes chronic inflammation, abnormal fibroblast proliferation, and collagen deposition while impeding epithelial migration. The extracellular polysaccharide matrix further limits antimicrobial penetration, exacerbating scar formation. Combined antibiofilm dressings, immunomodulation, and antifibrotic therapies may reduce scarring. To study bacterial colonization effects, we developed an animal model where subcutaneous bacterial injection induced inflammation specifically at the dermal reticular layer junction, bypassing traditional wounding methods. This effectively mimics folliculitis-related and idiopathic pathological scars. The model recapitulates key human scar features: erythematous/hyperpigmented appearance, tissue hardening, reduced mobility, and appendage loss, providing a platform for mechanistic studies and therapeutic development.

This study demonstrated bacterial colonization in pathological scar tissue through genetic, proteomic, morphological, and functional analyses. Following the clinical definition of colonization [50], we provide first evidence that bacteria persist in scar tissue, inhabiting both extracellular matrix and host cells while actively influencing

cellular behavior. Colonizing bacteria and their metabolites promote inflammation, alter proliferation, and dysregulate extracellular matrix deposition, ultimately driving scar hyperplasia. Our findings suggest that bacterial-induced chronic inflammation in the reticular dermis may initiate pathological scarring.

Conclusion

The presence of colonized bacteria within pathological scars continuously stimulates macrophages with the bacterial bodies and their secreted toxins, leading to local chronic. This results in the persistent activation of fibroblasts, which affects the clinical manifestations of pathological scars. We speculated that chronic inflammation in the dermal ret layer, caused by bacterial colonization, may be one of the initiating factors in pathological scar formation, which provide a potential new strategy for preventing and treating pathological scars.

Clinical perspectives

Pathological scars are regarded to be highly associated with chronic inflammation, whereas what factors contribute to this inflammation remains unclear. We found that the persistent inflammatory response mediated by macrophages due to bacterial colonization played an important role in pathological scar formation. This persistent inflammation affected the secretion of cytokines by macrophages, leading to dysregulated collagen secretion by fibroblasts and their transformation into myofroblasts through activating the TGF-β/Smad signaling pathway, resulting in the increasing of α-SMA, eventually leading to the formation of pathological scars. This research present new insights into the causes of pathological scars. Future research directions could include not only diagnostic approaches to detect bacterial colonization that triggers pathological scar formation through inflammatory activation, but also the development of targeted preventive or therapeutic interventions.

Abbreviations

TNF-α	Tumor necrosis factor-α
TGF-β	transforming growth factor-β
IL-1	interleukin-1
IL-6	interleukin-6
LB	Luria Broth
ATCC	American Type Culture Collection
RT-qPCR	real-time quantitative PCR
LTA	Lipoteichoic Acid
LPS	Lipopolysaccharide
PBS-MT	PBS containing 5% nonfat milk and 0.1% Tween 20
16S rRNA FISH	16S ribosomal ribonucleic acid fluorescence in situ hybridization
E	ear piercing
B	burns
I	infections
S	surgeries
T	trauma
S. aureus	Staphylococcus aureus
P. aeruginosa	Pseudomonas aeruginosa
K. pneumoniae	Klebsiella pneumoniae
P. acnes	Propionibacterium acnes

Supplementary Information

The online version contains supplementary material available at https://doi.org/10.1186/s12967-025-06585-1.

Supplementary Material 1

Acknowledgements

Special acknowledgement to the Figdraw platform, where the graphic abstract was drawn by it.

Author contributions

Ning Yang and Hao Zhang were responsible for clinical sample collection and experimental parts. Yuheng Zhang wrote the full text of this research. Bin Lin finished all the figures. Rong Huang and Tingting Cui modified the text and figures and provided funding support. Xueyong Li reviewed and finalized the research direction, performed the operations on all patients, and provided funding support.

Funding

This article was supported by National Natural Science Foundation of China (No. 82070282), Key Research and Development Program of Shaanxi Province, China (2024SF-GJHX-20), The Excellent Young Scientist Foundation of Xinjiang Uyghur Autonomous Region of China [2022D01E52].

Data availability

The data of sequencing was uploaded to the Sequence Read Archive (SRA) database (BioProject accession number: PRJNA811823; ID: 811823). Other data is provided within the manuscript file.

Declarations

Ethics approval and consent to participate

This study complied with the guidelines provided by the World Medical Association Declaration of Helsinki on Ethical Principles for Medical Research Involving Humans for studies, and was approved by the Ethics Committee of the Second Affiliated Hospital of Air Force Medical University (No. 202011-33 and 202201-02). All patients agreed to participate in this study and received test reports of their own samples.

Consent for publication

All authors have read and agree to publish this study.

Competing interests

The authors have declared that no competing interest exists.

Author details

[1]Department of Burn and Plastics Surgery, Tangdu Hospital, The Fourth Military Medical University, Xi'an 710038, China
[2]Department of Plastic and Burn Surgery, Joint Logistics Support Force of Chinese PLA, No. 927 Hospital, Puer 665000, China
[3]Department of Orthopedics, Western Theater Air Force Hospital of PLA, Chengdu 610011, China
[4]Department of Biochemistry and Molecular Biology, Preclinical Medicine College, Xinjiang Medical University, Urumqi 830011, China

Received: 11 January 2025 / Accepted: 7 May 2025
Published online: 21 May 2025

References

1. Zhu Z, Kong W, Wang H, Xiao Y, Shi Y, Gan L, et al. Clinical status of hospitalized keloid cases from 2013 to 2018. Burns. 2022;48(8):1874–84. https://doi.org/10.1016/j.burns.2021.12.007.

2. Ghazawi FM, Zargham R, Gilardino MS, Sasseville D, Jafarian F. Insights into the pathophysiology of hypertrophic scars and keloids: how do they differ. Adv Skin Wound Care. 2018;31(1):582–95. https://doi.org/10.1097/01.ASW.0000527576.27489.0f.
3. Liang Y, Zhou R, Fu X, Wang C, Wang D. HOXA5 counteracts the function of pathological scar-derived fibroblasts by partially activating p53 signaling. Cell Death Dis. 2021;12(1):40. https://doi.org/10.1038/s41419-020-03323-x.
4. Wang ZC, Zhao WY, Cao Y, Liu YQ, Sun Q, Shi P, et al. The roles of inflammation in keloid and hypertrophic scars. Front Immunol. 2020;11:603187. https://doi.org/10.3389/fimmu.2020.603187.
5. Dohi T, Padmanabhan J, Akaishi S, Than PA, Terashima M, Matsumoto NN, et al. The interplay of mechanical stress, strain, and stiffness at the keloid periphery correlates with increased Caveolin-1/ROCK signaling and Scar progression. Plast Reconstr Surg. 2019;144(1):e58–67. https://doi.org/10.1097/PRS.0000000000005717.
6. Sobec RL, Fodor L, Bodog F. Topical Oxandrolone reduces ear hypertrophic Scar formation in rabbits. Plast Reconstr Surg. 2019;143(2):481–7. https://doi.org/10.1097/PRS.0000000000005275.
7. Hong YK, Chang YH, Lin YC, Chen B, Guevara B, Hsu CK. Inflammation in wound healing and pathological scarring. Adv Wound Care (New Rochelle). 2023;12(5):288–300. https://doi.org/10.1089/wound.2021.0161.
8. Ogawa R. Keloid and hypertrophic scars are the result of chronic inflammation in the reticular dermis. Int J Mol Sci. 2017;18(3):606. https://doi.org/10.3390/ijms18030606.
9. Ogawa R, Dohi T, Tosa M, Aoki M, Akaishi S. The latest strategy for keloid and hypertrophic Scar prevention and treatment: the Nippon medical school (NMS) protocol. J Nippon Med Sch. 2021;88(1):2–9. https://doi.org/10.1272/jnms.JNMS.2021_88-106.
10. Li T, Chen W, Zhang Q, Deng C. Human-specific gene CHRFAM7A mediates M2 macrophage polarization via the Notch pathway to ameliorate hypertrophic Scar formation. Biomed Pharmacother. 2020;131:110611. https://doi.org/10.1016/j.biopha.2020.110611.
11. Zhao LT, Gao LM, Chen XD, Wu XY. A massive mandibular keloid with severe infection: what is your treatment. Photodiagnosis Photodyn Ther. 2021;33:102200. https://doi.org/10.1016/j.pdpdt.2021.102200.
12. Delaleu J, Duverger L, Shourick J, Tirgan MH, Algain M, Tounkara T, et al. Suppurative keloids: a complication of severe keloid disease. Int J Dermatol. 2021;60(11):1392–6. https://doi.org/10.1111/ijd.15641.
13. Maamouri R, Zaouak A, Ali A, Frioui R, Cheour M. Keloid Scar after herpes Zoster ophthalmicus. J Cosmet Dermatol. 2023;22(5):1704–5. https://doi.org/10.1111/jocd.15636.
14. Eley SJ, Carroll BT. Intralesional triamcinolone acetonide injection of keloid resulting in copious purulence. Dermatol Surg. 2023;49(6):628–9. https://doi.org/10.1097/DSS.0000000000003795.
15. Butzelaar L, Ulrich MM, van der Mink AB, Niessen FB, Beelen RH. Currently known risk factors for hypertrophic skin scarring: A review. J Plast Reconstr Aesthet Surg. 2016;69(2):163–9. https://doi.org/10.1016/j.bjps.2015.11.015.
16. Nejman D, Livyatan I, Fuks G, Gavert N, Zwang Y, Geller LT, Rotter-Maskowitz A, Weiser R, Mallel G, Gigi E, et al. The human tumor Microbiome is composed of tumor type-specific intracellular bacteria. Science. 2020;368:973–80.
17. Raetz CR, Whitfield C. Lipopolysaccharide endotoxins. Annu Rev Biochem. 2002;71:635–700. https://doi.org/10.1146/annurev.biochem.71.110601.135414.
18. Amann RI, Binder BJ, Olson RJ, Chisholm SW, Devereux R, Stahl DA. Combination of 16S rRNA-targeted oligonucleotide probes with flow cytometry for analyzing mixed microbial populations. Appl Environ Microbiol. 1990;56(6):1919–25. https://doi.org/10.1128/aem.56.6.1919-1925.1990.
19. Tang M, Kaymaz Y, Logeman BL, Eichhorn S, Liang ZS, Dulac C, Sackton TB. Evaluating single-cell cluster stability using the Jaccard similarity index. Bioinformatics. 2021;37:2212–4.
20. Finn DR. A metagenomic alpha-diversity index for microbial functional biodiversity. FEMS Microbiol Ecol. 2024;100:fiae019.
21. Konopiński MK. Shannon diversity index: a call to replace the original Shannon's formula with unbiased estimator in the population genetics studies. PeerJ. 2020;8:e9391.
22. Mascharak S, desJardins-Park HE, Davitt MF, Griffin M, Borrelli MR, Moore AL, et al. Preventing Engrailed-1 activation in fibroblasts yields wound regeneration without scarring. Science. 2021;372(6540):eaba2374. https://doi.org/10.1126/science.aba2374.
23. Ghazizadeh M, Tosa M, Shimizu H, Hyakusoku H, Kawanami O. Functional implications of the IL-6 signaling pathway in keloid pathogenesis. J Invest Dermatol. 2007;127(1):98–105. https://doi.org/10.1038/sj.jid.5700564.
24. Cheng SC, Huang WC, Pang S, Wu JH, Cheng YH. Quercetin inhibits the production of IL-1β-Induced inflammatory cytokines and chemokines in ARPE-19 cells via the MAPK and NF-κB signaling pathways. Int J Mol Sci. 2019;20(12). https://doi.org/10.3390/ijms20122957.
25. Campanati A, Goteri G, Simonetti O, Ganzetti G, Giuliodori K, Stramazzotti D, et al. CTACK /CCL27 expression in psoriatic skin and its modification after administration of etanercept. Br J Dermatol. 2007;157(6):1155–60. https://doi.org/10.1111/j.1365-2133.2007.08200.x.
26. Nishiguchi MA, Spencer CA, Leung DH, Leung TH. Aging suppresses Skin-Derived Circulating SDF1 to promote Full-Thickness tissue regeneration. Cell Rep. 2018;24(13):3383–e925. https://doi.org/10.1016/j.celrep.2018.08.054.
27. Duffield JS, Forbes SJ, Constandinou CM, Clay S, Partolina M, Vuthoori S, et al. Selective depletion of macrophages reveals distinct, opposing roles during liver injury and repair. J Clin Invest. 2005;115(1):56–65. https://doi.org/10.1172/JCI22675.
28. Komi D, Khomtchouk K, Santa Maria PL. A review of the contribution of mast cells in wound healing: involved molecular and cellular mechanisms. Clin Rev Allergy Immunol. 2020;58(3):298–312. https://doi.org/10.1007/s12016-019-08729-w.
29. Wulff BC, Parent AE, Meleski MA, DiPietro LA, Schrementi ME, Wilgus TA. Mast cells contribute to Scar formation during fetal wound healing. J Invest Dermatol. 2012;132(2):458–65. https://doi.org/10.1038/jid.2011.324.
30. Baker RH, Townley WA, McKeon S, Linge C, Vijh V. Retrospective study of the association between hypertrophic burn scarring and bacterial colonization. J Burn Care Res. 2007;28(1):152–6. https://doi.org/10.1097/BCR.0B013E31802CB860.
31. Errington J, Mickiewicz K, Kawai Y, Wu LJ. L-form bacteria, chronic diseases and the origins of life. Philos Trans R Soc Lond B Biol Sci. 2016;371(1707):20150494. https://doi.org/10.1098/rstb.2015.0494.
32. Byrd AL, Belkaid Y, Segre JA. The human skin Microbiome. Nat Rev Microbiol. 2018;16(3):143–55. https://doi.org/10.1038/nrmicro.2017.157.
33. Bik EM, Long CD, Armitage GC, Loomer P, Emerson J, Mongodin EF, et al. Bacterial diversity in the oral cavity of 10 healthy individuals. ISME J. 2010;4(8):962–74. https://doi.org/10.1038/ismej.2010.30.
34. Eckburg PB, Bik EM, Bernstein CN, Purdom E, Dethlefsen L, Sargent M, et al. Diversity of the human intestinal microbial flora. Science. 2005;308(5728):1635–8. https://doi.org/10.1126/science.1110591.
35. Bik EM, Eckburg PB, Gill SR, Nelson KE, Purdom EA, Francois F, et al. Molecular analysis of the bacterial microbiota in the human stomach. Proc Natl Acad Sci U S A. 2006;103(3):732–7. https://doi.org/10.1073/pnas.0506655103.
36. Fu A, Yao B, Dong T, Chen Y, Yao J, Liu Y, et al. Tumor-resident intracellular microbiota promotes metastatic colonization in breast cancer. Cell. 2022;185(8):1356–e7226. https://doi.org/10.1016/j.cell.2022.02.027.
37. Fan Y, Pedersen O. Gut microbiota in human metabolic health and disease. Nat Rev Microbiol. 2021;19(1):55–71. https://doi.org/10.1038/s41579-020-0433-9.
38. Tan S, Khumalo N, Bayat A. Understanding keloid pathobiology from a Quasi-Neoplastic perspective: less of a Scar and more of a chronic inflammatory disease with Cancer-Like tendencies. Front Immunol. 2019;10:1810. https://doi.org/10.3389/fimmu.2019.01810.
39. Mahmoudi S, Mancini E, Xu L, Moore A, Jahanbani F, Hebestreit K, et al. Heterogeneity in old fibroblasts is linked to variability in reprogramming and wound healing. Nature. 2019;574(7779):553–8. https://doi.org/10.1038/s41586-019-1658-5.
40. Van Linthout S, Miteva K, Tschöpe C. Crosstalk between fibroblasts and inflammatory cells. Cardiovasc Res. 2014;102(2):258–69. https://doi.org/10.1093/cvr/cvu062.
41. Vinaik R, Barayan D, Auger C, Abdullahi A, Jeschke MG. Regulation of Glycolysis and the Warburg effect in wound healing. JCI Insight. 2020;5(17):e138949. https://doi.org/10.1172/jci.insight.138949.
42. Kim J, Park JC, Lee MH, Yang CE, Lee JH, Lee WJ. High-Mobility group box 1 mediates fibroblast activity via RAGE-MAPK and NF-κB signaling in keloid Scar formation. Int J Mol Sci. 2017;19(1):76. https://doi.org/10.3390/ijms19010076.
43. Zhao W, Ma L, Cai C, Gong X. Caffeine inhibits NLRP3 inflammasome activation by suppressing MAPK/NF-κB and A2aR signaling in LPS-Induced THP-1 macrophages. Int J Biol Sci. 2019;15(8):1571–81. https://doi.org/10.7150/ijbs.34211.
44. Johnson BZ, Stevenson AW, Prêle CM, Fear MW, Wood FM. The role of IL-6 in skin fibrosis and cutaneous wound healing. Biomedicines. 2020;8:101.
45. Hata A, Chen YG. TGF-β signaling from receptors to Smads. Cold Spring Harb Perspect Biol. 2016;8(9). https://doi.org/10.1101/cshperspect.a022061.

46. Wang L, Wang HL, Liu TT, Lan HY. TGF-Beta as a master regulator of diabetic nephropathy. Int J Mol Sci. 2021;22(15):7881. https://doi.org/10.3390/ijms22157881.
47. Bautista-Hernández LA, Gómez-Olivares JL, Buentello-Volante B, Bautista-de Lucio VM. Fibroblasts: the unknown sentinels eliciting immune responses against microorganisms. Eur J Microbiol Immunol (Bp). 2017;7(3):151–7. https://doi.org/10.1556/1886.2017.00009.
48. Gäbele E, Dostert K, Hofmann C, Wiest R, Schölmerich J, Hellerbrand C, et al. DSS induced colitis increases portal LPS levels and enhances hepatic inflammation and fibrogenesis in experimental NASH. J Hepatol. 2011;55(6):1391–9. https://doi.org/10.1016/j.jhep.2011.02.035.
49. Shi J, Shi S, Xie W, Zhao M, Li Y, Zhang J, et al. IL-10 alleviates lipopolysaccharide-induced skin scarring via IL-10R/STAT3 axis regulating TLR4/NF-κB pathway in dermal fibroblasts. J Cell Mol Med. 2021;25(3):1554–67. https://doi.org/10.1111/jcmm.16250.
50. Schultz GS, Barillo DJ, Mozingo DW, Chin GA, Wound Bed Advisory Board Members. Wound bed Preparation and a brief history of TIME. Int Wound J. 2004;1(1):19–32. https://doi.org/10.1111/j.1742-481x.2004.00008.x.

Publisher's note